RADIO FREQUENCY FOREGROUND EMISSION AND THE SEPARATION OF MICROWAVE ANISOTROPIES FROM FOREGROUND CONTAMINATION

A.N. Lasenby
MRAO, Cavendish Laboratory
Cambridge, U.K.

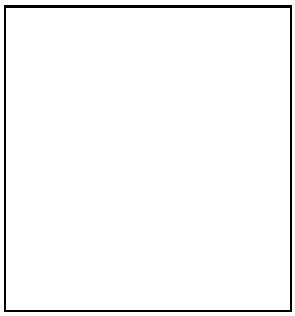

Abstract

The effects on CMB measurements of foreground contamination due to synchrotron radiation, free-free emission and discrete sources are considered. Estimates of the level and power spectrum of the Galactic fluctuations are made using low frequency maps and recent Tenerife data. New methods for achieving a frequency-based separation of Galactic and CMB components are discussed, and a positive/negative maximum entropy algorithm shown to be particularly powerful in this respect.

1 Introduction

A common feature of all current and future CMB experiments is that contamination of the CMB signal by foreground components must be dealt with. The most important contaminants over the frequency range of interest for the CMB are the effects of discrete radio and sub-mm sources, and the effects of our own Galaxy. Discrete sources can in principle be discriminated against on the basis of their quite different angular size compared to the CMB fluctuations of interest. For Galactic effects however, no such assumption can be made, and we must discriminate between them and CMB purely on the grounds of their differing behaviour with frequency.

In this context it is very important to have as good an estimate as we can of the likely level of Galactic anisotropies, and to be armed with good algorithms for separating out their effects. This is an area which will see great development over the next few years as we prepare for the

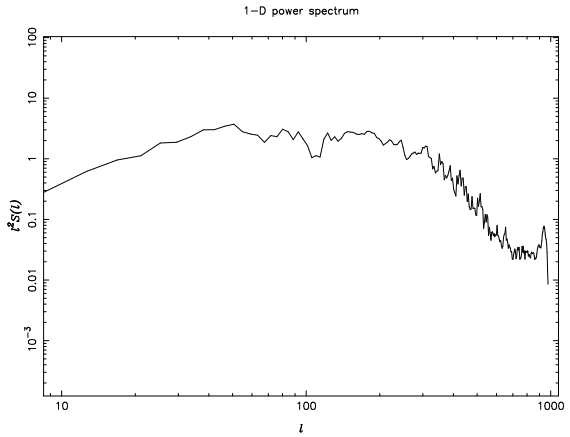

Figure 1: 1-d power 408 MHz spectrum for Tenerife patch

next generation of experiments, but as a preliminary effort in this direction we consider here, in schematic form, some recent estimates of Galactic variation gathered using current CMB experiments and low frequency maps. Data on a new type of discrete source whose spectrum can mimic a thermal source is also discussed. In the main part of the contribution, methods of performing the Galactic frequency separation are briefly reviewed, and the good performance for this purpose of a maximum entropy algorithm allowing both positive and negative fluctuations is highlighted.

2 Power spectrum and level of Galactic fluctuations

It is difficult to use the low frequency 408 MHz [6] and 1420 MHz [11] maps to extrapolate Galactic variations to CMB observing frequencies. The problems include difficulties with base-levels, scanning effects and of course with only two frequencies available only one spectral index can be estimated, whereas in principle the maps are mixtures of synchrotron and free-free emission, which have different spectral indices. As further problems, the synchrotron spectral index probably varies with frequency (on physical grounds it is expected to steepen with increasing frequency), and the maps are of a limited resolution (0.85° and 0.6° at 408 and 1420 MHz respectively) which makes it difficult to assess effects on scales below where the first Doppler peak is expected to lie for CMB fluctuations in an inflationary picture.

However, one thing we *can* use the low frequency maps for is to estimate the spatial power spectrum of high-latitude Galactic variations, at least on angular scales above the point where scanning effects and/or the limited resolution become significant. Figs. 1 and 2 (prepared by M.P. Hobson) show the 1-dimensional spatial power spectra at 408 and 1420 MHz for a patch of sky which has been extensively sampled by the 'Tenerife' experiments. The section used is 165° to 225° in Right Ascension and 35° to 45° in Declination. A Hanning window has been applied and an overall mean subtracted. The spectrum is given in terms of spherical multipole l and multiplied by l^2, so that it can be directly compared to the usual plots of CMB power — in particular, a scale invariant spectrum would have zero slope on this plot. It has recently been suggested, on a number of grounds, that the Galactic power spectrum behaves as l^{-3} as one approaches smaller angular scales [12]. The observational basis of this for dust emission seems well established, but the plots presented here favour a slightly less steep index for synchrotron emission (assuming this is the dominant component at 408 and 1420 MHz). In fact, the fall off at higher l away from an l^{-2} scale-invariant behaviour, begins in both plots at an angular scale which corresponds to the effects one would expect given the limited resolution of the maps.

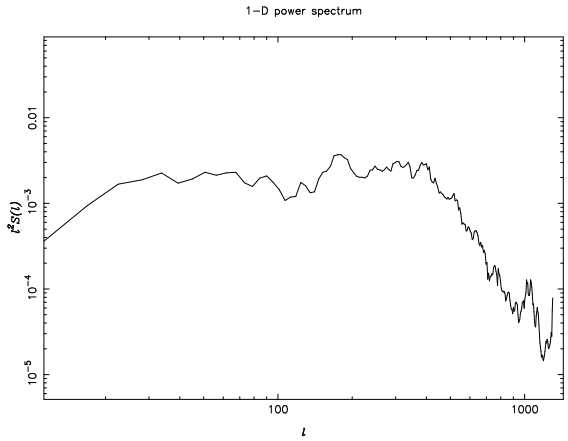

Figure 2: 1-d power 1420 MHz spectrum for Tenerife patch

In any case, these results make it clear that the Galactic foreground problem will not get any *worse* compared to the CMB levels as one goes to higher resolutions, and this is encouraging for future experiments.

2.1 Estimating the fluctuation level

The Tenerife experiments constitute a suite of three instruments, operating at 10, 15 and 33 GHz, on angular scales of $\sim 5^\circ$, and are therefore potentially well-suited to providing an estimate of the Galactic component on these scales. They were designed and built at Jodrell Bank [3, 4] and are operated by the IAC in-situ on Tenerife island. In fact, the level of anisotropy seen does not change very much in passing from 15 to 33 GHz [5] and this makes it difficult to assess the Galactic contribution, the implication being that the majority of the signal detected is CMB. However, we can set upper limits on the Galactic contribution as follows. Using the COBE DMR 2 year data and an assumed scale invariant CMB spectrum, we can predict a level of $31\,\mu$K that should be the *rms* observed in the Tenerife scans (at all frequencies since the beam geometry is the same at each frequency). We can then estimate other contributions to the signal (in particular the point source contribution) and then subtract in quadrature from the *observed rms* in order to obtain a residual, which can be interpreted as an estimate of the Galactic contribution. This process is shown in Table 1, with the result and 68% error bounds given in the row labelled 'residual'. In the next two rows, the predicted Galactic contribution

Component	10GHz signal μK	15GHz signal μK
Point sources	12.8	6.5
Signal	39^{+16}_{-14}	37^{+11}_{-8}
CMB pred. ($n = 1$)	31	31
Residual	24^{+22}_{-24}	20^{+16}_{-20}
1420 MHz $\beta = 2.75$	89	33
408/1420 MHz	185	76
β from 1420 MHz	3.4	3.0

Table 1: Breakdown of different contributions to the measured anisotropy in the Tenerife experiments at 10 and 15 GHz.

is shown assuming first a spectral index ($T \propto \nu^{-\beta}$) of $\beta = 2.75$ in going from 1420 MHz to

the Tenerife frequencies and secondly using the 408 and 1420 MHz maps themselves to provide the spectral index to use in the extrapolation. In the final row, the β necessary to get the residuals found starting from 1420 MHz is shown, and indicates a considerable steepening over the canonical 2.75 value. The area of sky included in generating these figures is the same as used for the power spectral plots shown above.

The fact that the residuals do not change too much between 10 and 15 GHz suggests that they do not represent a true Galactic level. (For example, even wholly free-free would reduce by a factor ~ 2.3 in passing from 10 to 15 GHz.) However, we could takes these numbers as 'worst case' levels. Thus, if we assume a free-free spectrum and take the numbers at 15 GHz, we can now predict the levels that will be seen in the COBRAS/SAMBA lower channels on the $\sim 5^\circ$ scale.

ν(GHz)	31.5	53	90
$\Delta T_{\rm Gal}(\,\mu$K)	$< 4^{+4}_{-4}$	$< 1.4^{+1.1}_{-1.4}$	$< 0.46^{+0.37}_{-0.46}$

We can compare these levels with the ($|b| > 20^\circ$) all-sky free-free levels suggested by Kogut's analysis (this volume) of the COBE DMR – DIRBE 140 μm cross-correlation:

ν(GHz)	31.5	53	90
$\Delta T_{\rm ff}(\,\mu$K)	21 ± 5	7 ± 2	2.3 ± 0.5

This suggests that the Tenerife region (approx 600 square degrees) is ~ 5 times better than average over the $|b| > 20^\circ$ sky. The availability of such large patches with relatively low Galactic levels is encouraging for future ground-based and balloon experiments, especially when coupled with the conclusion that things get no worse as one moves down in angular scale from the Tenerife/COBE scales.

3 Discrete sources

As mentioned above, discrete radio and sub-mm sources can be discriminated from CMB fluctuations via their quite different angular scale. This requires having higher resolution available than the resolution at which the CMB information is desired of course. As an example of how trying to eliminate radio sources using spectral information alone could go wrong, we show in Fig. 3 the spectrum of the source RXJ1459.9+3337 over the radio sub-mm region. (This figure and associated information were kindly provided by Alistair Edge.) The data are from multi-frequency VLA observations taken in April 1996 and JCMT photometry in May 1996. RXJ1459.9+333 is a quasar that was discovered first in X-rays, and only later measured as a radio source. The spectrum 'turns over' at a point somewhere between 20 and 40GHz, and on the rising side has a slope of ~ 1.8, virtually indistinguishable from the CMB over this range. Since the source was selected at X-ray, rather than on the basis of its radio properties, we do not how how rare such sources are — it would not have turned up in previous radio surveys. Some indication of the frequency of occurrence of such sources may come from another such source, slightly weaker, which was found serendipitously in a search of ~ 0.5 square degrees in a ROSAT cluster field using the Ryle Telescope at 15GHz. One such source in each ~ 0.5 square degrees area would not pose a formidable threat to CMB astronomy, but shows that we do have to be on our guard for the unexpected.

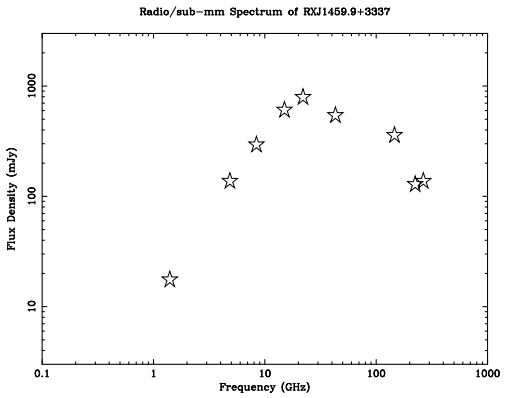

Figure 3: The radio/sub-mm spectrum for the X-ray selected quasar RXJ1459.9+3337. (Figure courtesy of A. Edge)

4 Algorithms for frequency separation

Methods for separating foreground contamination from the CMB include pixel by pixel separation using least squares [2], marginalization [7, 10], Wiener filtering [1, 12] and maximum entropy methods (MEM) [8, 9]. Here we wish to consider particularly the use of 2-channel (positive/negative) maximum entropy, which can simultaneously achieve both deconvolution and frequency separation.

The classical MEM approach to combining observations, and removing the effects of a switched beam etc., uses an assumption of positivity (e.g. White and Bunn [13]). The CMB sky, however, apart from an unobservable monopole, has zero mean and is expected to fluctuate equally between positive and negative. White and Bunn try to repair this by adding a positive constant to the data, but the need to include a default measure as well results in less space in which to reconstruct negative as opposed to positive features, and a consequent bias in the results. This may be verified by numerical simulations. Instead 2- channel MEM may be used, in which positive and negative channels are reconstructed simultaneously. This has been shown to work well in deconvolution of switched beam data [8] and avoids the problem with bias. Recently, Maisinger *et al.* [9] have applied this technique to foreground/CMB separation using multifrequency data in the context of simulated interferometer observations, and the results below are taken from that paper. This method can be contrasted with that of Wiener filtering. The latter provides the optimal linear method in the case that the power spectrum of the separate components is known. MEM is a non-linear method, which does not rely on any assumption about the power spectra, but just that the skies it reconstructs have the smallest information content consistent with the actual data.

The examples given in the following figures concentrate on the case of the VSA (see Jones, this volume). Two channels of data are used, at 28 and 38 GHz, each with bandwidth 2 GHz, with observations made for 30× 12 hours at each frequency. Fig. 4 shows the true (CDM) sky used in the simulation on the right, and its MEM reconstruction on the left. An important point which must be made is that the reconstruction can only be made within the sky area sampled by the telescope, and this is controlled by the circular primary beam. This is why the reconstruction fades to zero (the default) near the edges. In Fig. 5 the power spectrum recovered from the reconstructed map is shown together with the real power spectrum and errors estimated by Monte Carlo simulations. The real power spectrum of course deviates from the underlying ensemble CMB power spectrum since only the realization corresponding to the single sky patch used is available. Figs. 6 and 7 show the same but for an implementation of

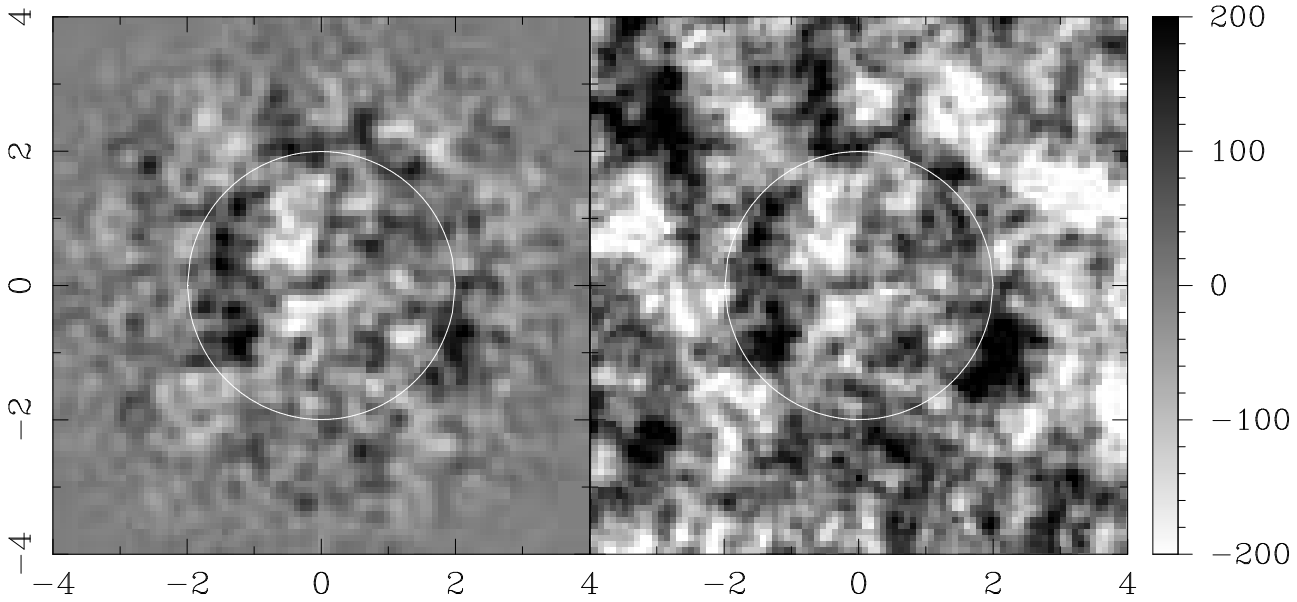

Figure 4: The MEM reconstruction of the CMBR component at 30 GHz in a $8^\circ \times 8^\circ$-field compared to the true underlying CMBR map used in the simulation. The grey-scales denote temperature fluctuations in μK. Neither of the maps is convolved with a synthesised beam, and the image is kept on the reconstruction grid. The circles indicate the FWHM of the primary telescope beam.

the Wiener filtering approach to this problem. Note in each case (MEM and Wiener), the true Galactic frequency spectral index used in the simulations ($\beta = 2.7$) is assumed known by the algorithm. However, it is not too difficult to relax this assumption, for example by including *two* channels for frequency reconstruction, each with a different assumed spectral index, and letting the algorithms decide how much weight to give each channel.

Overall it can be seen that this application of MEM is very successful, clearly outperforming the Wiener method in this case. We are investigating its use for frequency based foreground/CMB separation in a variety of other contexts also.

Acknowledgements. I am grateful to all the members of the CAT and Tenerife teams at Jodrell Bank and Cambridge for help with the preparation of material, particularly Mike Hobson, Stephen Hancock, Mike Jones, Klaus Maisinger, Carlos Gutiérrez and Aled Jones.

References

[1] F.R. Bouchet, R. Gispert and J.L. Puget, 1995, in E. Dwek, ed., Proceedings of the COBE workshop *"Unveiling the Cosmic Infrared Background"*, Baltimore, Maryland, USA

[2] W.N. Brandt, C.R. Lawrence, A.C.S. Readhead, J.N. Pakianathan and T.M. Fiola, 1994, *Ap J.*, 424, 1

[3] R.D. Davies, R.A. Watson, E.J. Daintree, J. Hopkins, A.N. Lasenby, J. Sanchez-Almeida, J.E. Beckman, and R. Rebolo, 1992, *Mon. Not. R. astr. Soc.*, 258, 605

[4] R.D. Davies, C.M. Gutiérrez, J. Hopkins, S. Melhuish, R.A. Watson, R. Hoyland, R. Rebolo, A.N. Lasenby, and S. Hancock, 1996, *Mon.Not.R.astr.Soc*, 278, 883

[5] S. Hancock, R.D. Davies, A.N. Lasenby, C.M. Gutiérrez, R.A. Watson, R. Rebolo, and J.E. Beckman, 1994, *Nature*, 367, 333

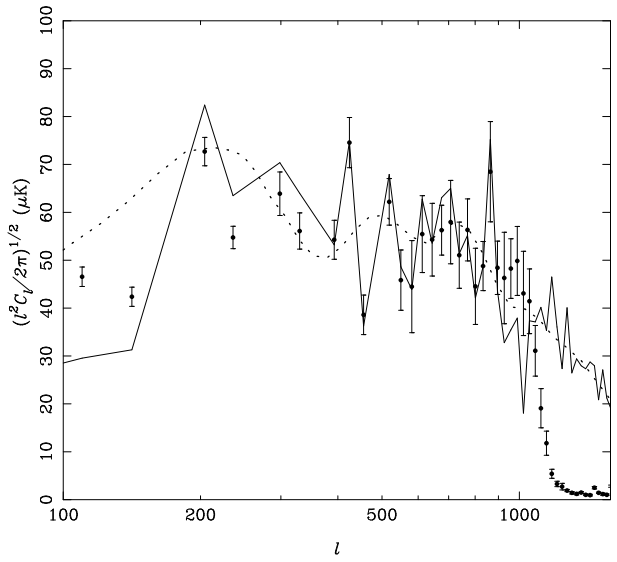

Figure 5: Comparison of power spectra of original (solid line) and reconstructed (points) CMBR maps. The error-bars indicate the 68-percent confidence limits as derived from 100 Monte-Carlo simulations with different noise realisations. Also plotted is the ensemble average CDM power spectrum (dotted line) from which the input map was generated.

[6] C.G.T. Haslam, C.J. Salter, H. Stoffel, and W.E. Wilson., 1982, *Astr. Astrophys. Suppl.*, 47, 1

[7] M.P. Hobson, A.N. Lasenby and M. Jones, 1995, *Mon. Not. R. astr. Soc.*, 275, 863

[8] A.W.Jones, S. Hancock, A.N. Lasenby, R.D. Davies, C.M. Gutiérrez, G. Rocha, R.A. Watson and R. Rebolo, 1996, *Mon. Not. R. astr. Soc.*, submitted

[9] K. Maisinger, M.P. Hobson and A.N. Lasenby, 1996, *Mon. Not. R. astr. Soc.*, submitted

[10] P.F. Scott *et al.*, 1996, *Ap J.*, 461, L1

[11] P. Reich and W. Reich, 1988, *Astr. Astrophys. Suppl.*, 74, 7

[12] M. Tegmark and G. Efstathiou, 1996, *Mon. Not. R. astr. Soc.*, in press

[13] M. White and E. Bunn, 1995, *Ap J.*, 443, L53

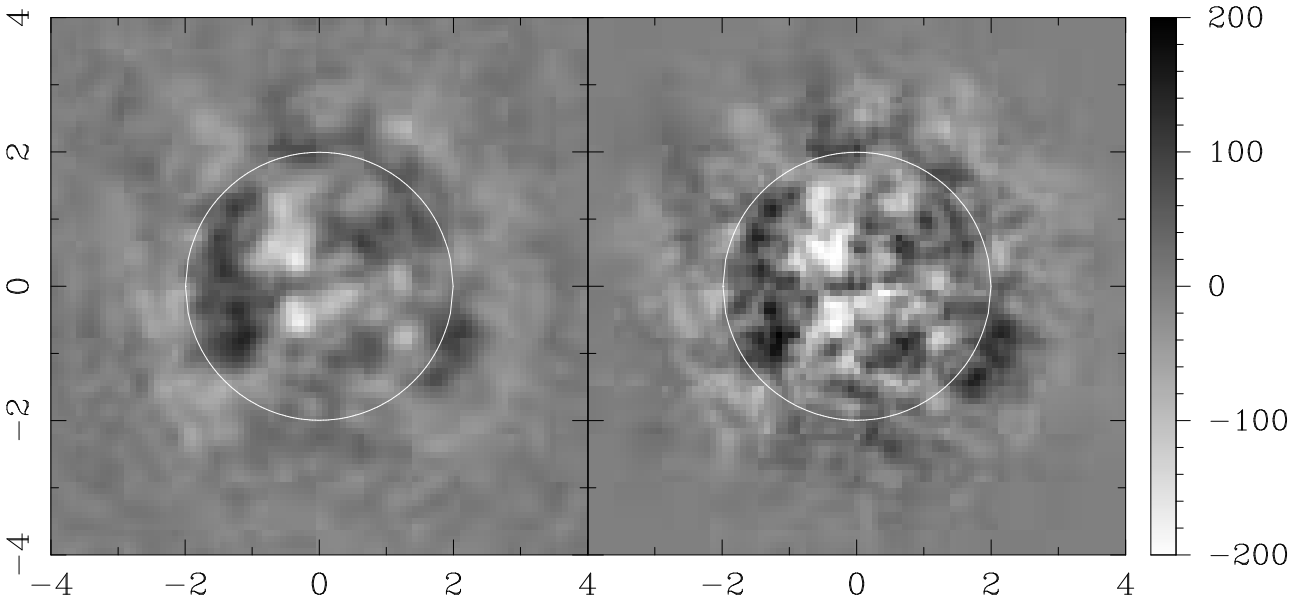

Figure 6: The Wiener filter reconstruction of the CMBR component at 30 GHz in a $8^\circ \times 8^\circ$-field compared to the true underlying CMBR map used in the simulation, multiplied by the primary beam. In contrast to Fig. 4, no deconvolution has been attempted in this case. The circles indicate the FWHM of the primary telescope beam.

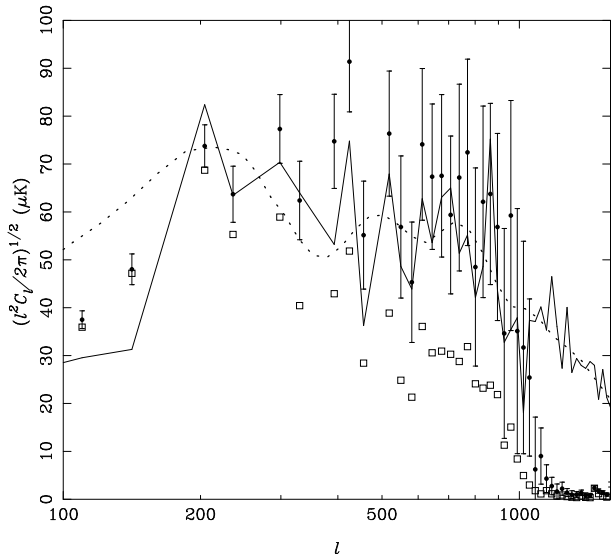

Figure 7: Comparison of power spectra of original (solid line) and reconstructed CMBR maps as obtained from linear filtering methods. Power spectra for both Wiener filtering (squares) and the rescaling method (dots) are plotted. Also plotted is the ensemble average CDM power spectrum (dotted line) from which the input map was generated.